RSC Advances

PAPER

Highly flexible solution processable heterostructured zinc oxide nanowires mesh for environmental clean-up applications

Cite this: *RSC Adv.*, 2014, **4**, 27481

Wei Li Ong,[a] Ken Wee Yew,[a] Chuan Fu Tan,[b] Teck Keng Tan Adrian,[b] Minghui Hong[a] and Ghim Wei Ho*[ab]

Received 30th April 2014
Accepted 9th June 2014

DOI: 10.1039/c4ra03951c

www.rsc.org/advances

We report the fabrication of a fully solution-processed ZnO nanowires array on flexible stainless steel mesh. ZnO nanowires of uniform dimensions are radially and densely assembled over a large area of the mesh. Various metal and metal oxide nanoparticles are photochemically deposited onto the ZnO nanowires and the corresponding effects on the photocurrent are investigated. Furthermore, the stability and robustness of the heterostructured ZnO nanowires grown on the mesh are evaluated by assessing the photocurrent in response to on/off cycles as well as undergoing various bending configurations. Finally, the heterostructured nanowire mesh is preliminarily tested for photodegradation of organic compound and separation of oil–water mixture. The multifunctional heterostructured nanowire mesh has shown potential applications for environmental clean-up purposes.

1. Introduction

Human activities have polluted aquatic environments with oil and dyes *via* both deliberate and accidental spills from a variety of industries, storage facilities and refineries. Hence, extensive research efforts on semiconductor materials have been devoted in response to environmental challenges such as oil–water separation and photocatalytic treatment of polluted water. Among the various semiconductor materials available, ZnO nanostructures possess many desirable attributes such as cheap, abundant, environmentally friendly, high quantum efficiency and UV light responsive.[1]

The photocatalytic performance of ZnO has been demonstrated and discussed in many reports.[2–4] However, its efficiency as a photocatalyst has been limited due to the recombination of photogenerated charge carriers that is typically faster than the production rate of reactive oxidation species. Thus, improving charge separation efficiency will require a rational design of the photocatalyst structure which can be achieved by coupling of ZnO with metal or metal oxide particles. The formed semiconductor–metal/metal oxide heterostructures aim to enhance the transfer of photogenerated charge carriers,[5,6] thereby reducing the recombination rate of electron–hole pairs. Noble metals are generally known to improve the photocatalytic activity of wide bandgap materials[7,8] due to the lower Fermi level of noble metals which facilitates electron transfer from ZnO to the loaded noble metal,[9] resulting in an efficient separation of charge carriers. Metal oxides such as copper oxide have also been shown to enhance photocurrent properties, providing a cheaper alternative to the expensive metal nanoparticles.[10,11]

Several synthesis methods of such hetero-nanostructures have been reported,[12,13] and amongst these methods, photochemical deposition which is based on the redox reactions of aqueous chemical species on photocatalytic solid surfaces, has the characteristics of site-specific growth on the target surface.[14] Moreover, this method has merits such as cost effectiveness, low processing temperature, and the possibility of being adapted for large-scale synthesis operations. Based on all these advantages, photochemical deposition is regarded as an excellent fabrication method for heterostructures. In addition, stainless steel mesh can be used as a cheaper alternative to traditional substrates such as fluorine-doped tin oxide (FTO) or indium-doped tin oxide (ITO). The wire mesh not only offers cost advantages, it also exhibits a larger effective surface area. Moreover, the mesh-like structure is anticipated to facilitate the separation of oil–water mixtures and also offers bigger spacing between the ZnO nanowires, resulting in optimal contact with the liquid medium of interest. Its flexibility also allows it to be folded into geometrical shapes that favor greater absorption of light. Finally, the material is able to withstand higher temperature compared to other flexible substrates.

However, there is limited development on functionalized flexible mesh that is not only durable and economical, but also possesses photocatalytic and separation capabilities. Herein, we report a low cost and fully solution processable ZnO heterostructured nanowire arrays on stainless steel mesh *via* facile

[a]*Department of Electrical and Computer Engineering, National University of Singapore, 4 Engineering Drive 3, 117583, Singapore. E-mail: elehgw@nus.edu.sg; Fax: +65 67754710; Tel: +65 65168121*

[b]*Engineering Science Programme, National University of Singapore, 9 Engineering Drive 1, 117575, Singapore*

hydrothermal and photochemical deposition methods. Photocurrents are measured on various heterostructured ZnO–Pt/Ag/CuO nanowire meshes to investigate their photoreactivity properties. Furthermore, the photoresponse stability and robustness of a bent heterostructured nanowire mesh is validated while retaining the excellent mechanical integrity of the underlying mesh. Finally, the heterostructured nanowire meshes are demonstrated for photodegradation and oil–water mixture separation associated to environmental clean-up applications.

2. Experimental

2.1 Synthesis of ZnO nanowires on stainless steel mesh

A 2 × 1.5 cm stainless steel wire mesh was ultrasonically cleaned in acetone, isopropyl alcohol (IPA) and deionized (DI) water. The mesh was then dipped into a ZnO colloidal solution prepared by dissolving 0.73 g of zinc acetate dihydrate ($Zn(CH_3COO)_2 \cdot 2H_2O$) and 0.37 g of potassium hydroxide (KOH) in 31 ml and 16 ml of methanol respectively. The zinc acetate precursor solution was placed in a water bath at 60 °C before the potassium hydroxide solution was added drop-wise and maintained for 1.5 h. A white precipitate was obtained, centrifuged and dispersed in 9 ml of butanol. The dip coated mesh was annealed at 350 °C for 10 min. The growth solution consisting of a 25 ml aqueous solution of 25 mM zinc nitrate hexahydrate ($Zn(NO_3)_2 \cdot 6H_2O$) and 50 mM hexamethylenetetramine (HMT) with 1 ml of 5 mM polyethylenimine (PEI) solution was prepared for growth of ZnO nanowires at 90 °C for 4 h. Finally, the sample was calcined at 450 °C in air for 30 min.

2.2 Loading with Pt, Ag, CuO nanoparticles

The reactant solutions for the loading of Pt, Ag and CuO nanoparticles were prepared by adding 5.11 mM of hexachloroplatinate(IV) hexahydrate ($H_2Cl_6Pt \cdot 6H_2O$), 9.27 mM silver nitrate ($AgNO_3$) or 15.74 mM copper(II) nitrate trihydrate ($Cu(NO_3)_2 \cdot 3H_2O$) solution to 20 ml of methanol respectively. The relevant solution with the nanowire mesh was transferred into a quartz tube and irradiated with a 300 W Xe arc lamp (Excelitas, PE300BFM) at an intensity of 1000 W m^{-2} for 1 h with constant magnetic stirring. 2 to 5 wt% of nanoparticles were loaded onto the ZnO nanowires.

2.3 Photocurrent measurements

1 × 1 cm meshes of various heterostructured nanowires were fabricated for a two-electrode configuration photocurrent measurement. ZnO nanowires meshes and Pt foil are used as the working and counter electrodes respectively with 25 mM anhydrous sodium sulphate (Na_2SO_4) as the electrolyte. The setup was exposed to a 300 W Xe arc lamp (intensity of 1000 W m^{-2}) and photocurrent measurements were carried out using a potentiostat (Princeton Applied Research, Parstat 4000) without applying potential bias.

2.4 Photodegradation of methyl orange

The photodegradation of methyl orange (MO) was performed in a quartz cylindrical reaction cell with the ZnO nanowires coated mesh (2 cm × 3.5 cm) vertically immersed in 15 ml of 0.015 mM MO aqueous solution. After keeping in the dark for 30 min to equilibrate, the sample was irradiated with a 300 W Xe arc lamp with constant stirring. The concentration of MO was determined using a UV-VIS-NIR spectrophotometer and the maximal absorbance peak value (at 462.5 nm) was noted to quantify the amount of MO remaining in solution and thus, determine the photodegradation activity of the nanowires. The residual dye content was calculated as C/C_0, where C and C_0 are concentrations of the tested and the original control solution (just after dark stirring), respectively.

2.5 Oil–water separation

The surface of the ZnO nanowires were chemically modified by immersing in 5 mM of stearic acid dissolved in ethanol for 24 h. The sample was then rinsed in ethanol and blown-dried with N_2 gas. The molecules formed a dense self-assembled monolayer on the ZnO surface as a result of the strong chelating bonds between the carboxylates and Zn atoms on the surface.[15] The hydrophobicity–oleophilicity of the treated mesh was tested with a mixture of oil and DI water (50% v/v). Vegetable oil was used as a substitute for environmental oil pollutant to demonstrate the oleophilicity of ZnO nanowires.

2.6 Materials characterization

Scanning electron microscopy (SEM, JEOL FEG JSM 7001F) operated at 15 kV was used to characterize the morphology of the synthesized ZnO heterostructured nanowires. The elements present in the nanostructures were analyzed using energy-dispersive X-ray spectroscopy (EDX, Oxford Instruments) and X-ray photoelectron spectroscopy (XPS) was employed to study the elemental composition of the nanoparticles loaded on the ZnO nanowires. The crystalline structures of the heterostructured nanowires were analyzed using transmission electron microscopy (TEM, Phillips FEG CM300) operated at 200 kV and X-ray diffraction (XRD, Philips X-ray diffractometer equipped with graphite-monochromated Cu Kα radiation at $\lambda = 1.541$ Å). Absorption spectra of the samples and MO were measured with a UV-VIS-NIR spectrophotometer (UV-VIS, Shimadzu UV-3600).

3. Results and discussion

The SEM image of the bare stainless steel mesh is shown in Fig. 1(a) and the inset shows the flexibility of the mesh. The ZnO nanowires coated mesh of different magnifications are shown in Fig. 1(b)–(d). It can be seen that there is a uniform coverage of nanowires on the mesh and the wires are relatively vertically-aligned. PEI was added to the growth solution to promote vertical orientation while hindering lateral growth of ZnO nanowires. Metal/metal oxide particles were then loaded on these ZnO nanowires by the photochemical deposition method. The SEM and TEM images of the samples are shown in Fig. 2. Fig. 2(a) shows an SEM image of Pt loaded ZnO nanowires. The

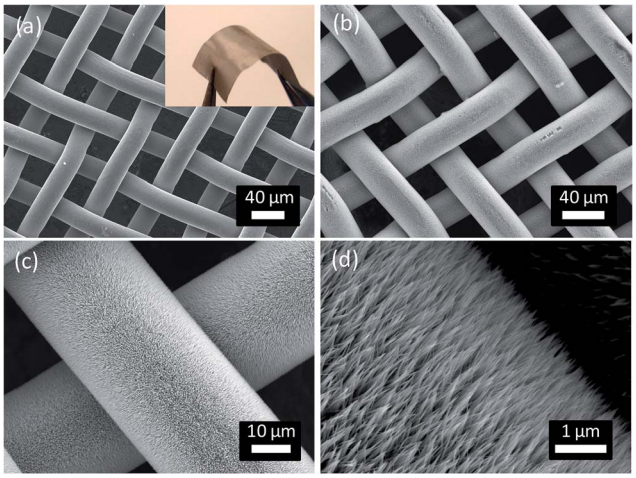

Fig. 1 SEM images of (a) bare mesh and (b–d) ZnO nanowires coated mesh at different magnifications. Inset of (a) shows a photograph of a flexible wire mesh.

Pt nanoparticles have an average diameter of about 2.5 nm, but were mostly agglomerated on the surface of the ZnO nanowires as shown in the corresponding TEM image (Fig. 2(b)). The Ag loaded ZnO nanowires are shown in Fig. 2(c) and (d). The SEM image (Fig. 2(c)) shows that the Ag particles are uniformly distributed on the nanowires and the TEM image shows that the average diameter is about 18 nm. Unlike Pt loading, no agglomeration of Ag nanoparticles was observed on the nanowires. The ZnO nanowires loaded with CuO nanoparticles were also characterized using SEM (Fig. 2(e)) and TEM (Fig. 2(f)). Loading of nanoparticles was not visible from the SEM image, however, small CuO nanoparticles with an average diameter of about 2.3 nm could be seen on the ZnO nanowires in the TEM image.

The loaded meshes were characterized using EDX and XRD (Fig. 3). Chromium (Cr), iron (Fe) and nickel (Ni) peaks observed in the EDX spectra for all the samples can be attributed to the stainless steel mesh. The presence of Pt and Ag nanoparticles was observed in EDX. However, Cu peak from the loaded CuO nanoparticles was not detected. This may suggest that the photodeposited CuO nanoparticles are too small and well-dispersed to be detected by EDX. XRD was also used to determine the crystallinity of the pristine and nanoparticles loaded ZnO nanowires. From the spectra in Fig. 3(b), peaks were observed at 31.8, 34.6, 36.4, 47.6, 56.7, 63.1 and 68.0° corresponding to the standard diffraction of (100), (002), (101), (102), (110), (103) and (112) planes of ZnO respectively (JCPDS card no. 79-0205). Peaks at 38.1 and 44.3° can be assigned to the (111)

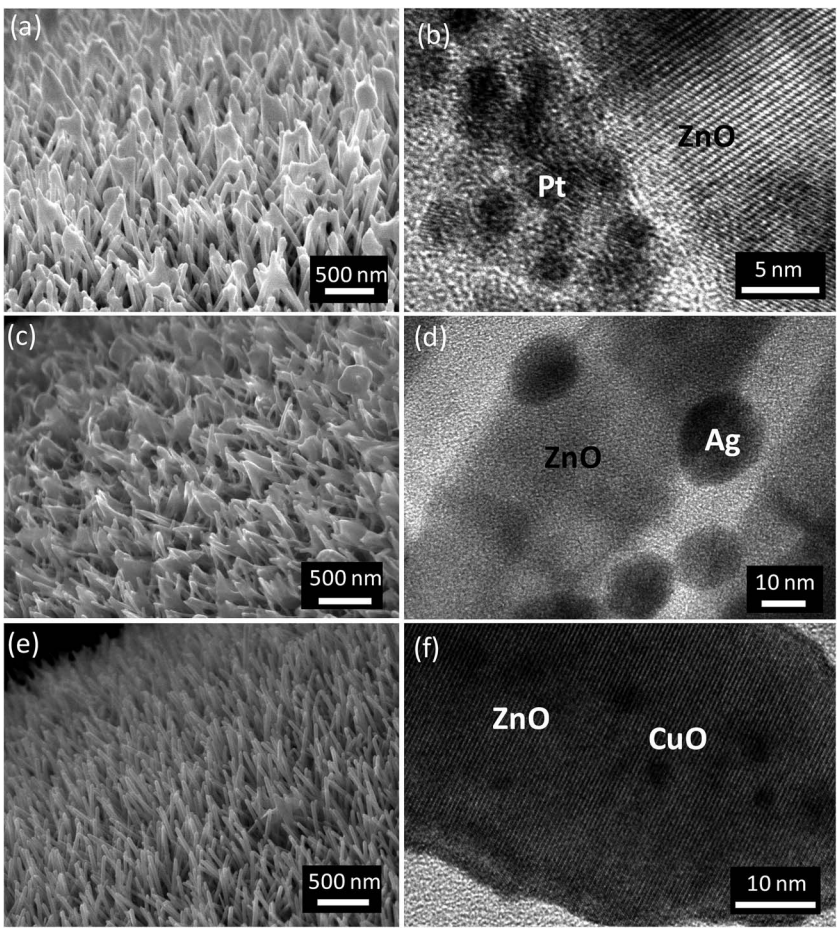

Fig. 2 SEM and TEM images of ZnO nanowires loaded with (a and b) Pt, (c and d) Ag and (e and f) CuO nanoparticles.

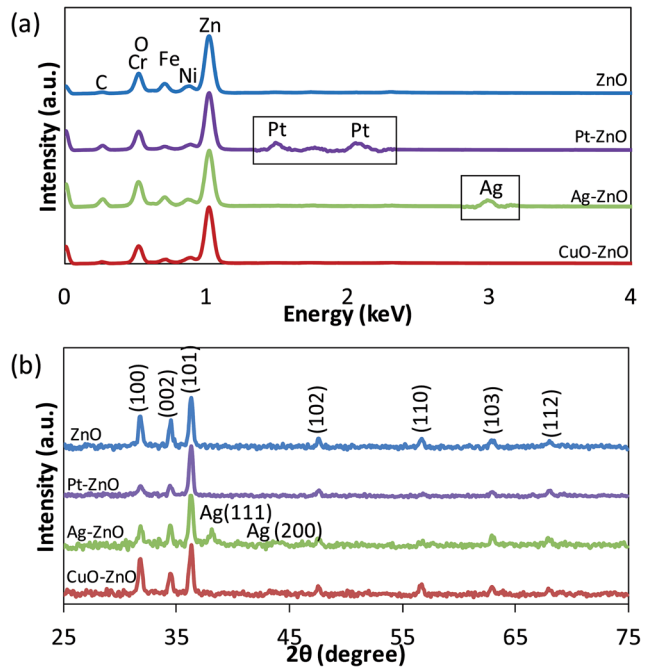

Fig. 3 (a) EDX and (b) XRD spectra of ZnO nanowires loaded with various nanoparticles. Insets of (a) show magnified (10×) views of Pt and Ag peaks.

and (200) planes of Ag (JCPDS card no. 65-2871). No peaks were observed for Pt and CuO, probably due to low loading of small diameter nanoparticles on the ZnO nanowires.

Hence surface sensitive XPS technique was used to detect the presence of the loaded nanoparticles and their respective oxidation states. The Pt 4f signals (Fig. 4(a)) obtained from the Pt nanoparticle could be deconvoluted into two pairs of doublets. The peaks centered at 71.2 and 74.6 eV are assigned to Pt $4f_{7/2}$ and Pt $4f_{5/2}$ respectively,[16] suggesting the presence of Pt nanoparticles on the ZnO nanowires. The other pair of doublets with peaks at 72.3 and 75.7 eV may be assigned to PtO.[17] The presence of PtO may be due to oxygen chemisorption on the Pt particle surface.[18] The peaks observed in Fig. 4(b) are attributed to Ag $3d_{5/2}$ (367.6 eV) and Ag $3d_{3/2}$ (373.6 eV), indicating the successful deposition of Ag nanoparticles on the ZnO nanowires. However, the binding energies of these peaks are noted to be lower than those of bulk Ag $3d_{5/2}$ (368.3 eV) and Ag $3d_{3/2}$ (374.3 eV).[19] This shift can be attributed to the strong interaction between metallic Ag nanoparticles and ZnO nanowires, where electrons are transferred from Ag to ZnO.[20,21] The Cu $2p_{3/2}$ and Cu $2p_{1/2}$ peaks are located at 934.6 and 954.4 eV respectively (Fig. 4(c)). These peaks along with the presence of the characteristic shakeup satellite peaks suggest that the copper oxidation state is +2 in the form of CuO nanoparticles,[22,23] and not metallic Cu or Cu_2O.

The absorbance of the heterostructured nanowires in the range of 300 to 800 nm were determined by UV-VIS absorbance measurements (Fig. 5(a)). There is a characteristic absorbance peak at 380 nm due to the bandgap of ZnO. All the heterostructured ZnO nanowires exhibit an increase in the visible light

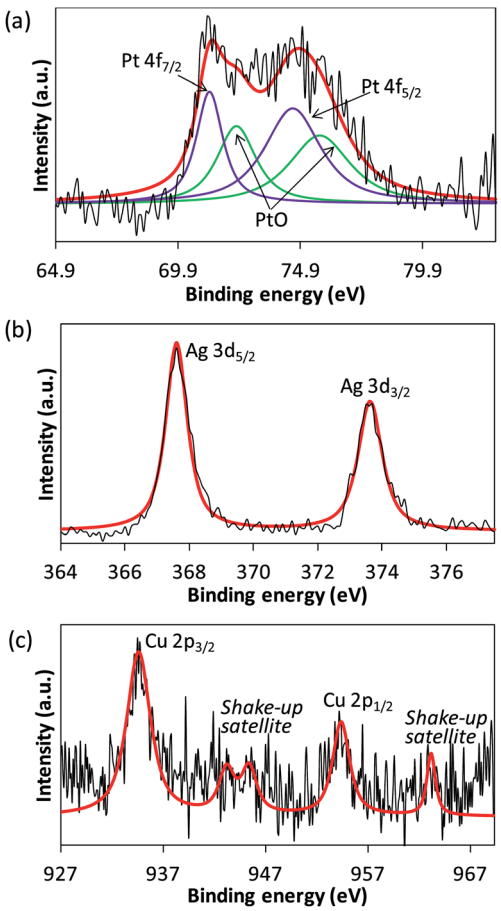

Fig. 4 XPS spectra of (a) Pt 4f, (b) Ag 3d and (c) Cu 2p.

absorption. The visible light absorption bands of CuO loaded ZnO nanowires might be due to excitation of CuO electrons from the valence band to the exciton level (<730 nm), and d–d

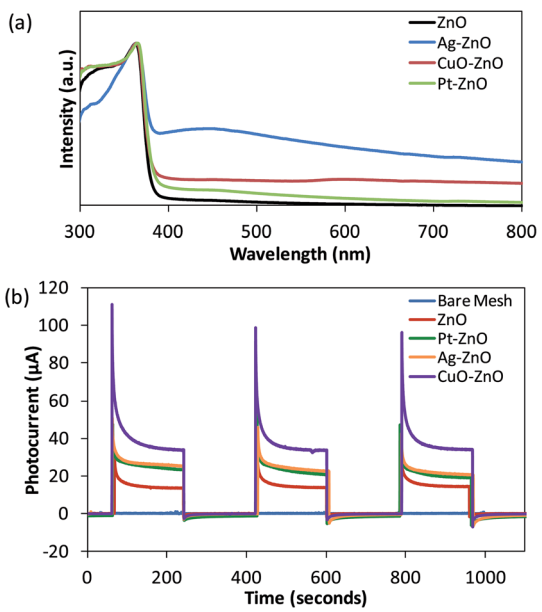

Fig. 5 (a) UV-VIS absorbance and (b) photocurrent measurements of ZnO nanowires loaded with various nanoparticles.

transition of Cu^{2+} (600–800 nm).[24] The highest absorbance was observed in the Ag loaded ZnO nanowires with a small peak at ~450 nm attributed to the surface plasmon resonance of the Ag nanoparticles.[25,26] The photocurrents measured from the pristine ZnO nanowires and samples loaded with various types of nanoparticles are shown in Fig. 5(b). The bare mesh did not produce any measurable photocurrent when exposed to light, but when ZnO nanowires were grown on the mesh, a photocurrent of 14.4 μA was measured. This indicates that the photocurrent measured is due to the generation of electron–hole pairs in ZnO nanowires. All the ZnO heterostructured nanowires were observed to perform better than the pristine ZnO nanowires. The CuO loaded ZnO nanowires showed the highest photocurrent of 34.2 μA while the Pt and Ag loaded nanowires produced photocurrents of 22.2 and 24.4 μA respectively. The improvement in the photocurrent output is mainly due to reduction of electron–hole pair recombination.[27] When ZnO nanowires are illuminated with light, the absorbed photon energy excites the electrons from the valence band to the conduction band.[28] However, since ZnO has a wide bandgap of 3.37 eV, only light with wavelengths shorter than or equal to 380 nm has sufficient energy to excite the electrons across the bandgap. Moreover, the excited electrons may also recombine with the holes due to presence of defects which act as recombination centers, resulting in low photocurrents.[29] However, with the addition of nanoparticles, the absorption of visible wavelengths increases, thus increasing the amount of electron–hole pairs generated and in turn the photocurrents. The metal/metal oxide nanoparticles also serve as electron reservoir to promote the separation of excitons and this reduces the rate of recombination, thus increasing the photocurrents.[27]

It has been reported that a higher Schottky barrier[30] between the metal nanoparticles and ZnO increases the efficiency of photogenerated electron transferring and trapping by the metal nanoparticles which leads to enhanced photocurrents. The work function of Ag is 4.74 eV,[31] and that of Pt nanoparticles is 5.93 eV,[31] while the work function of ZnO reported in literature is about 5.2 eV, with an electron affinity of 4.3 eV.[21] Though the higher Pt work function infers formation of a higher Schottky barrier, the photodeposited Pt nanoparticles are highly agglomerated which reduces the surface area available for photoreactivity.[32] As a result, the photocurrent obtained from the Ag loaded ZnO nanowires is higher than the Pt loaded ZnO nanowires. CuO loaded ZnO nanowires show the highest

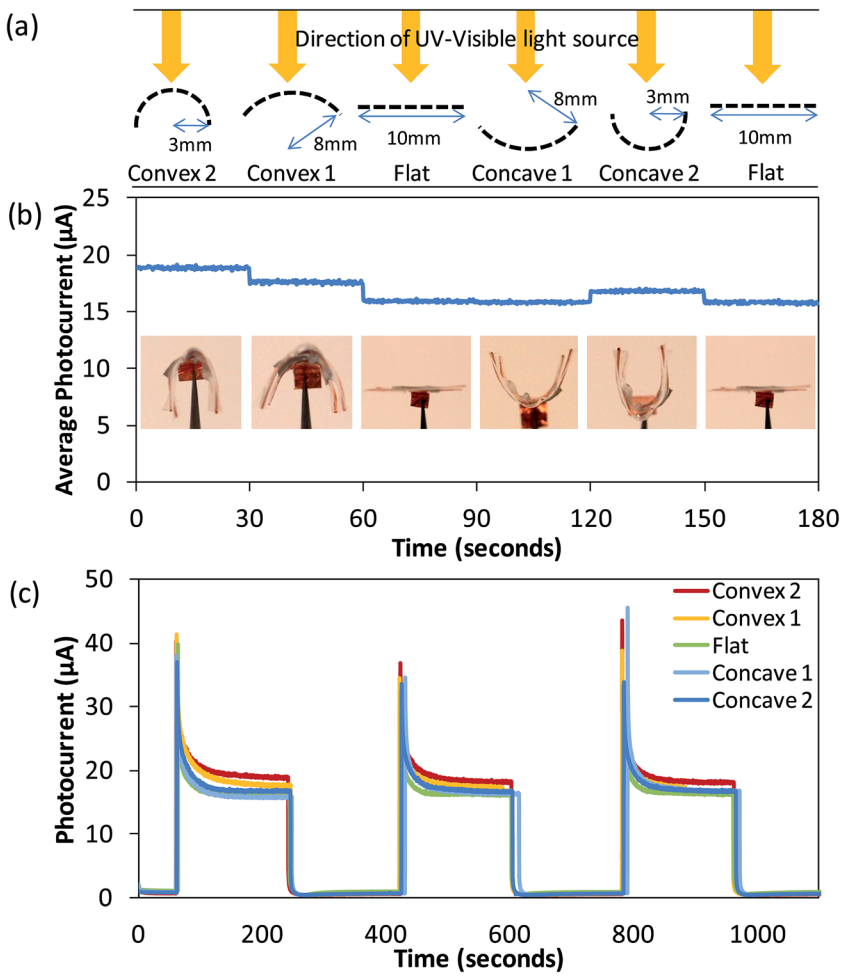

Fig. 6 (a) Schematic diagram illustrating the bending of ZnO nanowires on mesh. (b) Average photocurrents of ZnO nanowires with various degrees of bending. Insets show the sample with various degrees of bending. (c) Photocurrent measurements of various bent samples over time.

photocurrent enhancement which may be attributed to the deposition of the smallest (2.3 nm) and well-dispersed CuO nanoparticles. When semiconductor CuO nanoparticles loaded nanowires are illuminated with the Xe arc lamp, electron–hole pairs are generated in both semiconductor ZnO and CuO. Due to the alignment of the energy bands between ZnO and CuO, the photogenerated electrons will transfer from CB of CuO to that of ZnO, and the photogenerated holes will move in the opposite direction from VB of ZnO to that of CuO. This movement of charge carriers aids in a decrease of electron–hole recombination and contributes to higher photocurrents.[33]

The sample was then tested under bending and flexing to prove the robustness of the nanowires coated mesh. The photocurrent generated under illumination was measured while subjecting the flexible sample to a series of bending positions. The schematic diagram in Fig. 6(a) illustrates the degree to which the ZnO nanowires coated mesh is bent and the direction from which the mesh is illuminated by the light source. The insets in Fig. 6(b) show the photographs of the sample in the unbent and also convex and concave bent states. In general, the average photocurrent measured was observed to show a slight increase when the sample was bent (Fig. 6(b)) and the sample was fully functional and responsive to the repeated ON and OFF states of the illumination (Fig. 6(c)). The slight increase in the photocurrent of the bent sample may be attributed to the enhanced light trapping.[34] When the sample is in the concave bent state, the incident light may be scattered and reflected multiple times on the surface of the bent sample. Compared with that on a flat sample, this multiple reflection helps to reduce the reflectivity loss.[34] When the sample is in the convex bent state, not only does the incident light illuminate the nanowires on the side of the sample facing the light, but also some of the light passes through the holes in the mesh and illuminates on the nanowires grown on the backside of the mesh. As a result, the photocurrents recorded from the bent samples are slightly higher than the flat sample.

The photodegradation capability of ZnO nanowires meshes on organic compounds was then investigated using MO as the model compound. The pristine ZnO nanowires and CuO loaded ZnO nanowires were studied in this experiment and the time profiles of the decrease in MO concentration are shown in Fig. 7(a). A control experiment was carried out to show that no appreciable photodegradation was observed in the absence of a photocatalyst. The pristine ZnO nanowires mesh required 5 h of illumination to completely degrade the MO molecules. In contrast, the MO dye was fully degraded by the CuO loaded ZnO nanowires mesh within 2 h. This enhancement in photodegradation activity is due to the CuO loaded ZnO exhibiting a higher photocatalytic performance than pristine ZnO nanowires, which is in agreement with the trend observed in Fig. 5. The pseudo-first order kinetics of the MO degradation was also computed and shown in Fig. 7(b). The efficiency of MO photodegradation can be determined using the pseudo-first order model[35] as follows:

$$\ln(C_0/C_t) = kt \quad (1)$$

where C_0 and C_t are the concentrations of dye at time 0 and t, respectively and k is the pseudo-first order rate constant. From the rate constant, k, shown in Fig. 7(b), the pristine ZnO nanowires has a constant of 0.0107 min^{-1} and CuO loaded ZnO has a constant of 0.0354 min^{-1}. The corresponding correlation coefficient, R^2, for the pristine ZnO and CuO loaded ZnO are 0.8936 and 0.9507 respectively. The results clearly demonstrate that the ZnO nanowires mesh loaded with CuO nanoparticles exhibits enhanced photodegradation over pristine ZnO mesh.

Besides photodegradation of organic compounds, the ZnO nanowires mesh is also preliminarily shown to separate oil and water mixture after surface treatment with stearic acid. As shown in Fig. 7(c) and (d), when the mixture was poured onto the mesh, the oil permeated through the mesh and dripped into the collecting bottle while the water was repelled by the mesh

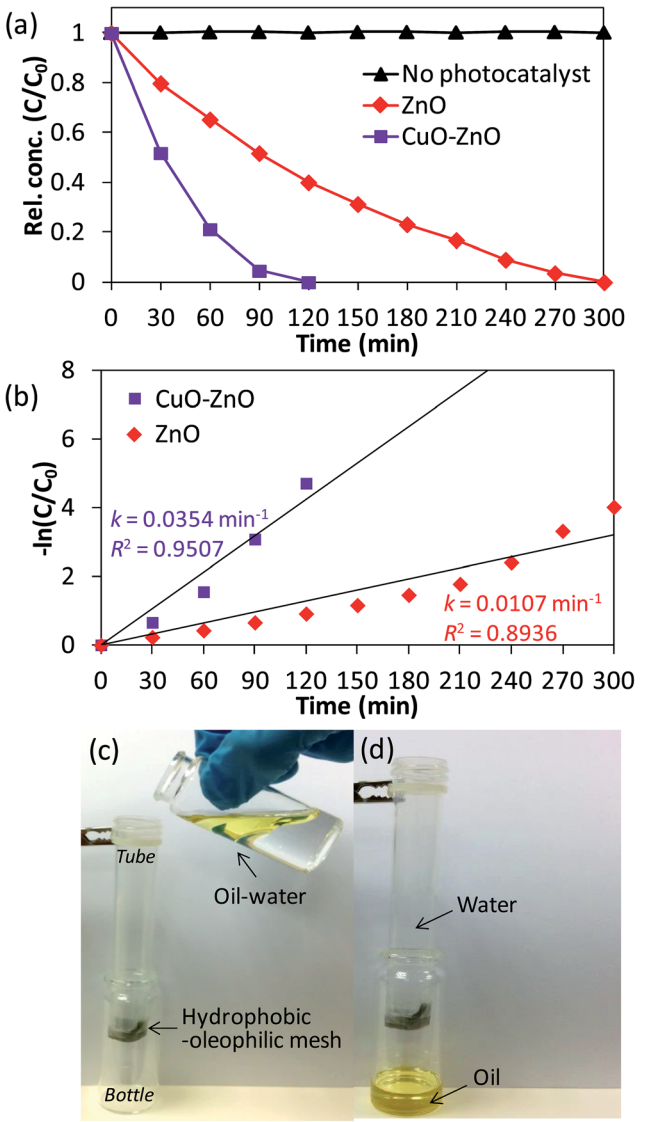

Fig. 7 (a) Degradation kinetics and (b) pseudo-first order kinetics of a time evolution MO photodegradation study in the absence and presence of pristine ZnO nanowires and CuO loaded ZnO nanowires. Demonstration of oil and water separation process; (c) before and (d) after separation.

and retained in the separating tube. The hydrophobic and oleophilic properties of the surface treated ZnO nanowires mesh is brought about by the long carbon chains of stearic acid on ZnO.[36] Stearic acid is known as a wax-like saturated fatty acid, so when stearic acid molecules are absorbed onto the ZnO nanowires, the surface free energy is lowered resulting in a hydrophobic surface.

4. Conclusions

ZnO nanowires were synthesized on a flexible stainless steel mesh by a simple and low temperature hydrothermal method. Photocurrents were measured on various heterostructured ZnO–Pt/Ag/CuO nanowire meshes to investigate their photoreactivity properties. The pristine ZnO nanowires shows a photocurrent of 14.4 μA while Pt, Ag and CuO loaded ZnO nanowires show enhanced photocurrents of 22.2, 24.4 and 34.2 μA respectively. The enhancement may be attributed to improved absorbance in the visible wavelength and also the reduction of electron–hole pair recombination. The photoresponse stability and robustness of the heterostructured nanowire mesh is proven with various bending configurations and cyclability. In relation to environmental clean-up applications, the ZnO nanowires mesh is capable of photocatalytically degrading MO, with the CuO loaded ZnO nanowires completing the photodegradation more efficiently than the pristine ZnO nanowires. Moreover, the nanowire mesh shows oil–water separation capability after surface treatment with stearic acid which tuned the nanowires towards hydrophobic–oleophilic characteristics.

Acknowledgements

This work is supported by A*STAR R-263-000-A96-305 and National Research Foundation (NRF) grant R-263-000-684-281.

References

1 W. L. Ong, S. Natarajan, B. Kloostra and G. W. Ho, *Nanoscale*, 2013, **5**, 5568–5575.
2 F. Xu, P. Zhang, A. Navrotsky, Z.-Y. Yuan, T.-Z. Ren, M. Halasa and B.-L. Su, *Chem. Mater.*, 2007, **19**, 5680–5686.
3 Y. Wang, X. Li, N. Wang, X. Quan and Y. Chen, *Sep. Purif. Technol.*, 2008, **62**, 727–732.
4 A. I. Inamdar, S. H. Mujawar, V. Ganesan and P. S. Patil, *Nanotechnology*, 2008, **19**, 325706.
5 J. H. Park, S. Kim and A. J. Bard, *Nano Lett.*, 2006, **6**, 24–28.
6 X. Y. Yang, A. Wolcott, G. M. Wang, A. Sobo, R. C. Fitzmorris, F. Qian, J. Z. Zhang and Y. Li, *Nano Lett.*, 2009, **9**, 2331–2336.
7 M. Ni, M. K. H. Leung, D. Y. C. Leung and K. Sumathy, *Renewable Sustainable Energy Rev.*, 2007, **11**, 401–425.
8 Z. K. Zheng, B. B. Huang, X. Y. Qin, X. Y. Zhang, Y. Dai and M. H. Whangbo, *J. Mater. Chem.*, 2011, **21**, 9079–9087.
9 A. L. Linsebigler, G. Q. Lu and J. T. Yates, *Chem. Rev.*, 1995, **95**, 735–758.
10 W. Q. Fan, Q. H. Lai, Q. H. Zhang and Y. Wang, *J. Phys. Chem. C*, 2011, **115**, 10694–10701.
11 Z. Chen, N. Zhang and Y. J. Xu, *CrystEngComm*, 2013, **15**, 3022–3030.
12 S. Y. Bae, H. W. Seo, H. C. Choi, J. Park and J. Park, *J. Phys. Chem. B*, 2004, **108**, 12318–12326.
13 S. W. Jung, W. I. Park, G. C. Yi and M. Y. Kim, *Adv. Mater.*, 2003, **15**, 1358–1361.
14 Y. Tak and K. Yong, *J. Phys. Chem. C*, 2007, **112**, 74–79.
15 C. F. Wang, Y. T. Wang, P. H. Tung, S. W. Kuo, C. H. Lin, Y. C. Sheen and F. C. Chang, *Langmuir*, 2006, **22**, 8289–8292.
16 M. Ahmad, L. Gan, C. Pan and J. Zhu, *Electrochim. Acta*, 2010, **55**, 6885–6891.
17 J. Després, M. Elsener, M. Koebel, O. Kröcher, B. Schnyder and A. Wokaun, *Appl. Catal., B*, 2004, **50**, 73–82.
18 C. Y. Su, Y. C. Hsueh, C. C. Kei, C. T. Lin and T. P. Perng, *J. Phys. Chem. C*, 2013, **117**, 11610–11618.
19 J. F. Moulder, W. F. Stickle, P. E. Sobol and K. D. Bomben, *Handbook of X-Ray Photoelectron Spectroscopy: A Reference Book of Standard Spectra for Identification and Interpretation of Xps Data*, Physical Electronics, Boston, 1995.
20 Y. Zheng, L. Zheng, Y. Zhan, X. Lin, Q. Zheng and K. Wei, *Inorg. Chem.*, 2007, **46**, 6980–6986.
21 W. Lu, S. Gao and J. Wang, *J. Phys. Chem. C*, 2008, **112**, 16792–16800.
22 S. Jung, S. Jeon and K. Yong, *Nanotechnology*, 2011, **22**, 015606.
23 Z. Liu, H. Bai, S. Xu and D. D. Sun, *Int. J. Hydrogen Energy*, 2011, **36**, 13473–13480.
24 H. Praliaud, S. Mikhailenko, Z. Chajar and M. Primet, *Appl. Catal., B*, 1998, **16**, 359–374.
25 K. C. Lee, S. J. Lin, C. H. Lin, C. S. Tsai and Y. J. Lu, *Surf. Coat. Technol.*, 2008, **202**, 5339–5342.
26 Y. Wei, J. Kong, L. Yang, L. Ke, H. R. Tan, H. Liu, Y. Huang, X. W. Sun, X. Lu and H. Du, *J. Mater. Chem. A*, 2013, **1**, 5045–5052.
27 J. W. Chiou, S. C. Ray, H. M. Tsai, C. W. Pao, F. Z. Chien, W. F. Pong, C. H. Tseng, J. J. Wu, M. H. Tsai, C. H. Chen, H. J. Lin, J. F. Lee and J. H. Guo, *J. Phys. Chem. C*, 2011, **115**, 2650–2655.
28 A. Wolcott, W. A. Smith, T. R. Kuykendall, Y. Zhao and J. Z. Zhang, *Adv. Funct. Mater.*, 2009, **19**, 1849–1856.
29 P. Thiyagarajan, H.-J. Ahn, J.-S. Lee, J.-C. Yoon and J.-H. Jang, *Small*, 2013, **9**, 2341–2347.
30 P. V. Kamat, *J. Phys. Chem. B*, 2002, **106**, 7729–7744.
31 D. R. Lide, *CRC Handbook of Chemistry and Physics*, Taylor & Francis, 87th edn, 2006.
32 Y. Zhang, J. Xu, P. Xu, Y. Zhu, X. Chen and W. Yu, *Nanotechnology*, 2010, **21**, 285501.
33 S. Wei, Y. Chen, Y. Ma and Z. Shao, *J. Mol. Catal. A: Chem.*, 2010, **331**, 112–116.
34 Y. F. Wei, L. Ke, J. H. Kong, H. Liu, Z. H. Jiao, X. H. Lu, H. J. Du and X. W. Sun, *Nanotechnology*, 2012, **23**, 235401.
35 J. M. Herrmann, H. Ahiri, Y. Ait-Ichou, G. Lassaletta, A. R. Gonzalez-Elipe and A. Fernandez, *Appl. Catal., B*, 1997, **13**, 219–228.
36 X. Wu, L. Zheng and D. Wu, *Langmuir*, 2005, **21**, 2665–2667.